Agricultural and Forest Meteorology 223 (2016) 72–80

Contents lists available at ScienceDirect

Agricultural and Forest Meteorology

journal homepage: www.elsevier.com/locate/agrformet

Spatio-temporal variability of erosivity estimated from highly resolved and adjusted radar rain data (RADOLAN)

Franziska Fischer[a,b,c], Julia Hauck[a], Robert Brandhuber[b], Elmar Weigl[d], Harald Maier[c], Karl Auerswald[a,*]

[a] Lehrstuhl für Grünlandlehre, Technische Universität München, Alte Akademie 12, 85354 Freising, Germany
[b] Bavarian State Research Center for Agriculture, Lange Point 6, 85356 Freising, Germany
[c] Deutscher Wetterdienst, Außenstelle Weihenstephan, Alte Akademie 16, 85354 Freising, Germany
[d] Deutscher Wetterdienst, Zentrale, Frankfurter Straße 135, 63067 Offenbach/Main, Germany

ARTICLE INFO

Article history:
Received 23 October 2015
Received in revised form 24 March 2016
Accepted 31 March 2016
Available online 13 April 2016

Keywords:
RADOLAN
Erosive rain
Rainfall erosivity
Spatio-temporal variability

ABSTRACT

Rainfall events exhibit high spatio-temporal variability and cause soil erosion when thresholds of rainfall amount or intensity are exceeded. Analogously high variability in space and time is assumed for erosivity (R). RADOLAN, from the German Weather Service, provides radar rainfall data at high spatio-temporal resolution (1×1 km^2, 5 min), adjusted in 60 min intervals by measurements from a dense rain-gauge network that potentially could overcome present limitations of R estimations from sparse rain gauges. This new database was used to analyse the spatio-temporal variability of rain depth and R for single events (event R) which occurred in an area of ~15 000 km^2 in southern Germany over a period of two years to illustrate the need for such high spatio-temporal resolution in rain data for R estimations. Further, the effect of calibrating 5 min resolved radar data using hourly adjustment factors to rain-gauge data was explored. The spatial gradients of event R were steep, even steeper than for rain intensity, and call for such highly resolved data. Erosivity exhibited a clear maximum late in the afternoon. Daily rainfall differed from erosive rainfall due to rain breaks and rain extending over more than one day. Event R between adjacent 1 km^2 cells differed by up to 120 N h^{-1}. Even on an annual scale, erosivity at grid cells not further than 10 km apart could differ by more than a factor of five. Adjustment of the rain data was indispensable when calculating event R because adjustment could change event R by a factor of two. Even if long-term averages are used, differences by lacking adjustment would not be levelled. RADOLAN thus provides, for the first time, rain data as required in distributed erosion modelling for time periods shorter than 20 years.

© 2016 Elsevier B.V. All rights reserved.

1. Introduction

Rainfall varies in space and time and drives many processes in nature. This is most obvious for rainfall–runoff relations (e.g. Bronstert and Bárdossy, 2003; Faurès et al., 1995; Kirkby et al., 2005) or soil erosion processes (e.g. Wischmeier and Smith 1958; Nearing, 1998). Several studies have investigated how the spatial variability of rainfall on scales >100 km^2 can be better estimated by improving the interpolation of rain-gauge points, optimizing rain-gauge networks or downscaling of remote sensing data, especially ground based radar measurements (Borga, 2002; Datta et al., 2003; Kruizinga and Yperlaan, 1978; Quirmbach and Schultz, 2002; Syed et al., 2003; Tsanis et al., 2002; Yang and Yu, 2015). Spatial variability is especially large for erosive rains that mainly result from convective rain cells. The diameter of rain cells may vary between 1 and 20 km primarily depending on wind shear (Malkowski, 1965) and rainfall intensities (Gryschka et al., 2008). Life spans range mainly between 15 and 35 min (Weusthoff and Hauf, 2008) but may be as long as 10 h, during which traveling distances of several 100 km may occur (Malkowski, 1961). Accordingly, rainfall erosivity exhibits high spatio-temporal variation (Da Silva et al., 2013; Fiener and Auerswald, 2009; Sadeghi et al., 2011). Data obtained from rain gauges were interpolated with methods like inverse distance weighting (Sadeghi et al., 2011) or kriging (Fiener and Auerswald, 2009; Lu and Yu, 2002; Sideris et al., 2014) but the use of spatio-temporally highly resolved radar rain has been proposed

Abbreviations: E, kinetic energy; I_{max30}, maximum 30 min rain intensity; RADOLAN, Radar OnLine-ANeichung (on-line adjusted radar); R, long-term average annual erosivity; R_e, event erosivity; R_{year}, annual sum of erosivity.

* Corresponding author.
E-mail address: auerswald@wzw.tum.de (K. Auerswald).

http://dx.doi.org/10.1016/j.agrformet.2016.03.024
0168-1923/© 2016 Elsevier B.V. All rights reserved.

to overcome the limitations of these interpolations and, in particular, for the determination of erosivity and erosion modeling (Cruse et al., 2006).

The German Weather Service (Deutscher Wetterdienst DWD, Offenbach) has set up 17 ground-based radar stations with a detection radius of maximal 150 km forming the RADOLAN network (Bartels et al., 2004; Weigl, 2011) that delivers rain intensity data with a spatial resolution of $1 \times 1\,km^2$ which is higher than its American equivalent NEXRAD (Next-Generation Radar; $\sim 16\,km^2$ resolution; Crum et al., 1998; Cruse et al., 2006; Hardegree et al., 2008). RADOLAN should thus be better suited to capturing the small-scale variation of rain cells. Furthermore, in RADOLAN the hourly rainfall data are immediately adjusted to ground-truth data from a network of 1300 rain gauges (Bartels et al., 2004) (on average about 250 stations per radar considering the overlap of radars) which improves estimation (Seo et al., 2010; Weigl and Winterrath, 2009). The acronym RADOLAN resolves to RAdar OnLine-ANeichung equivalent to on-line adjusted radar. While adjustment is carried out hourly (called RW data in RADOLAN), the highest temporal resolution of the radar intensity data is 5 min (RY data in RADOLAN). This temporal resolution combined with adjustment may yield rain erosivity similar to that obtained from rain-gauge data. RADOLAN thus may offer, for the first time, data at a spatio-temporal resolution and an accuracy to calculate maps of rain erosivity for single rain events.

We used RADOLAN data to explore the spatio-temporal variability of rain erosivity in an area of 86 km × 181 km during a two-year period. In particular, we investigated (i) whether the temporal resolution of 5 min is short enough for the calculation of erosivity, (ii) what effect the adjustment for 1 h increments has, (iii) how erosive-rain properties vary diurnally, (iv) how the erosivity cells are spatially structured, which determines the spatial requirements of rain measurement, and finally (v) to what degree the spatial structure of individual erosive rains is attenuated by aggregation to annual and biennial erosivities.

2. Material and methods

2.1. Rainfall data and processing

In the Universal Soil Loss Equation USLE and its many modifications and successors, long-term average rain erosivity is quantified in the *R* factor (Wischmeier and Smith, 1958). It is calculated as the mean annual sum of the event erosivities. Event erosivity in turn is calculated as the product of the kinetic energy (E) and the maximum 30 min rain intensity (I_{max30}). Event erosivity is thus often termed *EI* or *EI30* but we will use R_e for event erosivities and R_{year} for annual sums for a specific year and R for the long-term average annual sum:

$$R_e = E \times I_{max30} \quad (1)$$

While in the USA and other countries often the unit MJ mm $ha^{-1}\,h^{-1}$ is used, we use $N\,h^{-1}$ for R_e, as it is the most commonly used unit of R in Europe and because of its simplicity. Both units can easily be converted by multiplying the values in $N\,h^{-1}$ with a factor of 10 to yield MJ mm $ha^{-1}\,h^{-1}$.

Erosive events are defined as rains that deliver more than 12.7 mm of rain or have a $I_{max30} \geq 12.7\,mm\,h^{-1}$ (Wischmeier and Smith, 1978). For the area under consideration, these thresholds have been lowered to 10 mm and $10\,mm\,h^{-1}$ (Rogler and Schwertmann, 1981). We will use these lower thresholds because all other factor values of the USLE, which have been derived from soil loss measurements in Germany since then, were calculated with these thresholds. These factor values will only remain applicable without adjustments by maintaining these thresholds. Different events are separated by rain breaks of more than 6 h (Wischmeier and Smith, 1978). Thus, up to three erosive rains are possible per day but an erosive rain can also last for several days.

Kinetic energy increases with rain intensity. Hence, kinetic energy (E) in $kJ\,m^{-2}$ for 1 mm of rain is calculated from

$$E = (11.89 + 8.73 \times \log I) \times 10^{-3} \text{for } 0.5\,mm\,h^{-1} \leq I \leq 76.2\,mm\,h^{-1} \quad (2a)$$

$$E = 0 \text{ for } I < 0.05\,mm\,h^{-1} \quad (2b)$$

$$E = 28.33 \times 10^{-3} \text{ for } I \geq 76.2\,mm\,h^{-1} \quad (2c)$$

and summed up over the entire erosive rain (Wischmeier and Smith, 1978). This set of equations produces similar results to the set of equations used in RUSLE2 (Foster, 2008) but we will compare USLE and RUSLE2 equations and the influence of the deviating German thresholds for our specific data set.

For the analysis of erosive rainfall events based on RADOLAN, we used the "RY data" at 5 min resolution from two years (2011 and 2012). The RY data are quality controlled including the correction of orographic shading, refined relationship of radar reflectivity to rainfall rate (Z/R) and clutter removal (Hengstebeck et al., 2010). The "RW data" is the hourly sum of RY that is adjusted to rain-gauge measurements at 60 min resolution by complex procedures (Bartels et al., 2004). We adjusted the 5 min RY data by assuming that the same correction factor can be applied for all 12 5-min increments in one hour. This correction factor was taken from the RW data at 60 min resolution.

2.2. Test site

The research area (Fig. 1) spanned 181 km by 86 km and covered 15566 grid cells of $1 \times 1\,km^2$ in polar stereographic projection. Except for a small part in the north-eastern corner, it was located in the Bavarian Tertiary Hills of southern Germany (48°13′N, 11°19′E – 48°52′N, 13°57′E), a landscape with pronounced soil erosion (Auerswald et al., 2009). The long-term mean annual R factor within this landscape is expected to vary little from 70 to $80\,N\,h^{-1}\,a^{-1}$ (Auerswald, 2006).

2.3. Data analysis

In total, 170 days during 2011 (81 days) and 2012 (89 days) met the criteria of an erosive rain event on at least one of the 15 566 grid cells. These days will be called erosive days. The magnitude and timing of the rainfalls differed among the grid cells (with many grid cells without erosive rain). We will therefore regard every erosive rain, which occurred in one grid cell, to be an erosive event.

The RY data cannot resolve intensity within the 5 min segments, which will influence the calculation of kinetic energy according to Eq. (2) but also the identification of I_{max30}. To quantify the effect of the temporal resolution on the calculation of kinetic energy and subsequently on R_e we used data from eight erosive rains given in Fiener and Auerswald (2009), which covered a wide range of magnitude. They were obtained from tipping-bucket rain gauges at a measuring resolution of 0.1 mm. These data were aggregated into temporal increments of 1 and 5 min. R_e was estimated from the data at both temporal resolutions to quantify the smoothing effect with decreasing resolution.

The assumption that the hourly adjustment also applies for the 5 min increments may lead to incorrect calculations of kinetic energy and I_{max30}. To quantify the effects of this adjustment, daily rain depth, kinetic energy, I_{max30} and R_e were estimated from original RY data and with RY data that were adjusted to preserve hourly

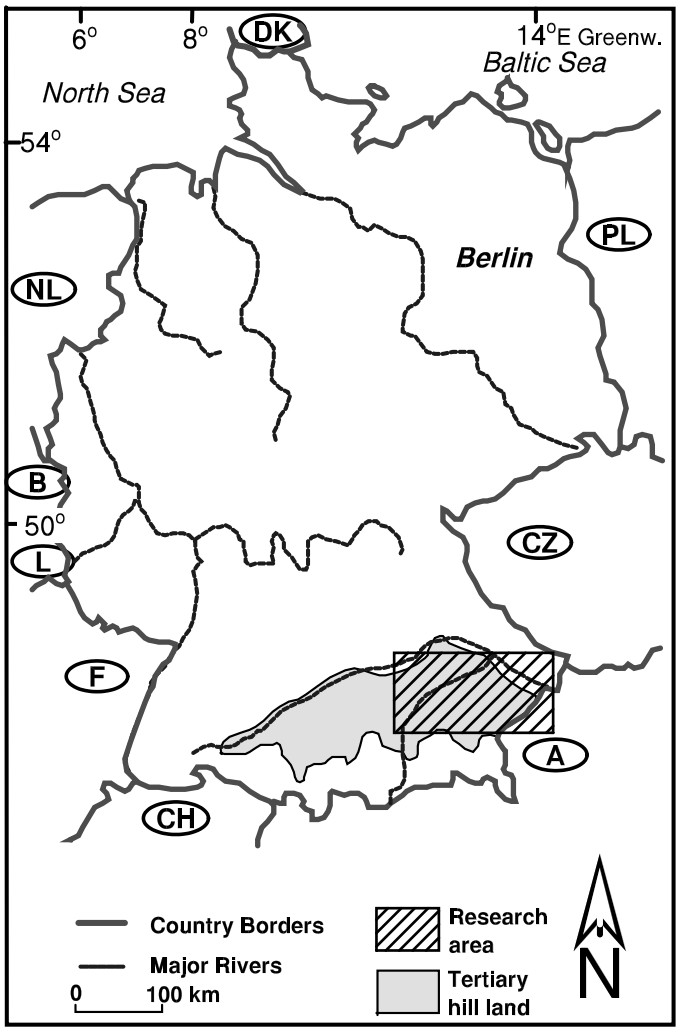

Fig. 1. Position of the research area (hatched rectangle) in the Tertiary hills in southern Germany.

rain-gauge measurements. Both results were compared for a subset of 93 456 events. Only grid cells with $R_e > 0$ were considered in this comparison.

In order to validate the adjusted RY data, we compared these data to rain-gauge data from 30 stations in 2011 and 29 stations in 2012 within our research area. These rain gauges were run by a different authority (Bavarian State Research Center for Agriculture) and their data were not used in RADOLAN calculations at any stage.

2.4. Diurnal variation of erosive-rain properties

Weather data are usually arbitrarily split into days where the break is locally defined. In the research area precipitation data are usually split at 7:30 Central European Time (Wohlrab et al., 1992) but the break could be at midnight or any other defined time. RADOLAN provides continuous data. Here we split days at 00:00 Coordinated Universal Time (UTC), which corresponds to 01:00 Central European Time. To estimate the need to consider dry spells >6 h within erosive days, the occurrence of these dry spells was determined.

All erosive days were pooled to determine the diurnal pattern of intensity and the occurrence of I_{max30}. To derive the diurnal pattern of intensity, all intensities within a 120-min window were combined and the maximum intensities were characterized by determining the 98 percentile. Then the window was moved by 5 min and the analysis was repeated. To derive the diurnal pattern of I_{max30}, the central time of each I_{max30} period was determined and the probability of I_{max30} to occur at a certain time of the day was then calculated by kernel density estimation (Silverman, 1986). Because of the cyclic nature of diurnal variation, we repeated the same data before and after one day to assure correct density estimation at the domain boundaries.

2.5. Spatial structure of erosive rains

The spatial structures of daily rain depth, kinetic energy, I_{max30}, R_e and R_{year} were quantified by semivariograms using *gstat* (Pebesma, 2004) in R version 3.1.0 (R Development Core Team, 2014). The data of most erosive days were strongly skewed. Data normalization was not carried out because this would have reduced the weight of high erosivity cells, which are most important regarding erosion. Spherical or Gaussian models were fitted to the experimental semivariograms by minimizing weighted least squares. For the Gaussian models, the true range was obtained by multiplication of the range parameter with sqrt(3), so that their range is comparable with the range of the spherical models (Journel and Huijbregts, 1978). Many semivariograms exhibited a hole effect indicating cell structures. In these cases spherical or Gaussian models were fitted to all lag classes until the maximum semivariance was reached. Finally, many semivariograms consisted of nested structures (e.g., high erosivity cells within large rain fields). In these cases only the short-distance structure that likely results from rain cells was used for fitting the semivariogram model to derive the nugget, partial sill and range. The weight was according to the number of point pairs divided by the squared distance. For convenience of comparison with the parameter under focus (e.g. calculation of the coefficient of variation), the square root of the semivariance (standard deviation) will also be reported. Anisotropy was quantified as relative difference between the isotropic and the directional (with directions differing by 45°) ratios of partial sill to range. In addition to the ratios of partial sill and range (i.e. the mean gradient within the range of autocorrelation), local gradients were calculated within 1.4 km (i.e., between an individual grid cell and all eight adjacent grid cells). The mean local gradient and the maximum local gradient to one of the eight neighbors were calculated and averaged over all grid cells.

3. Results

3.1. Rain characteristics of erosive days

In 2011 and 2012, 19.5 d a^{-1} with erosive rains were identified per grid cell, but considering the entire research area and both years there was a total of 170 days for which at least one of the grid cells had an erosive rain. Days with erosive rains on at least one grid cell occurred from April to December with most events from May to August (Table 1). The rains lasted between 0.3 h to 19 h (averages of monthly minimum and maximum values) but the duration within an individual day varied largely depending on the grid cell (e.g., from 1 to 11 h with a mean of 5 h on 24 Aug 2011). Daily rain depth varied between the erosive days from less than 5 mm d^{-1} up to 124 mm d^{-1}, but again there was a large spatial variation between the grid cells within individual days (e.g., from 7 mm d^{-1} to 72 mm d^{-1} with a mean of 15 mm d^{-1} on 31 May 2012). Considering only erosive events, kinetic energy of the rain ranged from 0.1 kJ m^{-2} to 3.2 kJ m^{-2}, with strong variation within the single days (e.g., from 0.05 kJ m^{-2} to 1.7 kJ m^{-2} with a mean of 0.4 kJ m^{-2} on 31 May 2011). I_{max30} of erosive events varied among the days between 1 mm h^{-1} and 192 mm h^{-1} and it also varied pronouncedly within single days (e.g. on 24 Aug 2011 from 6 mm h^{-1} to 107 mm h^{-1} with

Table 1
Characteristics of all erosive days in 2011 and 2012: number of erosive days per month; minimum (min), mean and maximum (max) of the number of grid cells per erosive day with $R_e > 0$ relative to the total area (15 566 grid cells); min, mean and max of erosive rain event duration, daily erosive rain depth, kinetic energy of erosive rains, maximum 30 min intensity (I_{max30}) and event erosivity (R_e) of grid cells with $R_e > 0$.

Parameter		Jan	Feb	Mar	Apr	May	June	July	Aug	Sept	Oct	Nov	Dec
Erosive days		0	0	0	4	24	33	36	30	14	8	6	15
Grid cells with $R_e > 0$ per erosive day (%)	Min				0.4	0.4	0.8	0.6	0.7	2.4	2.8	2.1	0.4
	Mean				18.1	15.3	28.2	19.2	28.9	23.4	30.3	28.5	15.0
	Max				52.2	94.3	97.5	99.0	94.2	77.3	67.1	88.2	59.7
Erosive rain duration (h)	Min				0.3	0.1	0.1	0.1	0.1	0.5	0.8	0.1	0.7
	Mean				4.5	3.8	5.0	4.0	5.1	7.6	8.1	8.2	8.4
	Max				11.5	18.0	16.8	23.3	23.7	22.3	22.8	18.8	19.3
Daily rain depth (mm d^{-1})	Min				5.4	5.1	5.0	5.0	5.0	5.3	5.6	10.0	5.7
	Mean				12.6	12.2	13.1	13.4	14.4	13.1	12.7	13.4	13.0
	Max				34.8	71.5	88.3	78.5	124.2	46.4	43.4	39.6	40.0
Kinetic energy (kJ km^{-2})	Min				0.1	0.1	0.1	0.1	0.1	0.1	0.1	0.1	0.1
	Mean				0.2	0.2	0.3	0.3	0.3	0.2	0.2	0.2	0.2
	Max				0.8	1.9	2.1	2.1	3.2	1.1	1.2	0.7	0.6
I_{max30} (mm h^{-1})	Min				2.9	2.3	1.6	1.8	1.5	1.4	1.0	1.7	1.0
	Mean				9.4	12.8	11.8	14.0	12.1	7.9	6.5	5.1	6.1
	Max				32.7	116.6	86.6	127.7	192.0	64.1	81.8	24.2	20.5
R_e (N h^{-1})	Min				0.4	0.3	0.2	0.3	0.2	0.1	0.1	0.2	0.1
	Mean				2.2	3.7	3.6	4.9	4.3	2.0	1.5	1.1	1.3
	Max				25.8	217.4	122.7	261.4	621.8	64.9	97.8	8.3	9.1

a mean of 23 mm h^{-1}). The variation of these parameters resulted in a variation of R_e between 0.1 N h^{-1} and 622 N h^{-1}. Again, the spatial variation within each erosive day was large (e.g. from 1 N h^{-1} to 206 N h^{-1} with a mean of 11 N h^{-1} on 24 Aug 2011).

During individual erosive days, rain occurred on average on about 90% of the research area, but the rain met the criteria of an erosive event only on a mean of 24% of the research area. The number of grid cells with an erosive event and hence the spatial extension of the erosive rainfalls varied strongly between erosive days from 1% to 99% of the entire research area. All erosive days and grid cells with erosive rain comprised a total data set of 605 737 erosive events.

Point rainfall measured by independent rain gauges (0.03 m^2) was similar to areal rainfall measured by radar (1 km^2). For all rains in 2011 and 2012 where point and areal measurements were both available (n = 11 292), the mean difference was only 4%. The RMSE between both measurements was 3 mm.

The USLE erosivity was on average 4% higher than the RUSLE2 erosivity, while the RMSE was 9%. The influence of the lower German thresholds was larger. On average this lead to 14% higher biennial erosivities and long-term averages may be adjusted accordingly. In particular, the difference can only occur for low rains and hence the difference occurred mainly at the edges of the erosive cells (see below), which would be even smaller and the spatial heterogeneity larger if the higher thresholds would have been applied. On average, the lower thresholds increased the number of grid cells that met the criteria of erosive rains by 7.5%.

3.2. Effect of temporal resolution

R_e estimated from the tipping-bucket rain gauges ranged from 1 N h^{-1} to 46 N h^{-1}. Lower temporal resolution of the rain data decreased kinetic energies, I_{max30} and R_e but the effect was small for a resolution of 5 min, as used for the RY data. The regression coefficients with 1-min resolution data were only slightly smaller than 1 for kinetic energy (slope 0.9903, $r^2 = 0.9999$), I_{max30} (slope 0.9929, $r^2 = 0.9999$) and R_e (slope 0.9845, $r^2 = 0.9999$).

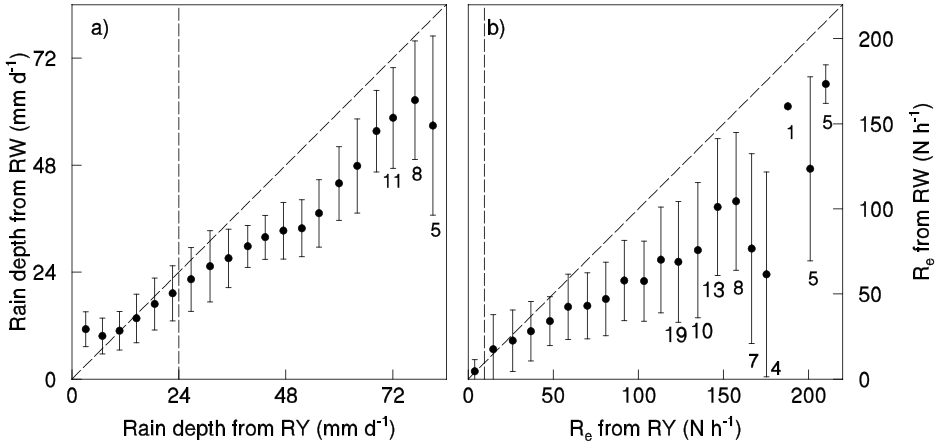

Fig. 2. Daily rain depth (a) and R_e (b) derived from (unadjusted) RY and (adjusted) RW data for 93 456 erosive events of 19 typical days (grid cells with $R_e = 0$ were omitted in the left panel to allow comparison between rain depth and R_e). Markers represent mean values of 20 subgroups (equidistant on x-axis) with bars of one SD. For means calculated from less than 20 value pairs, the number of value pairs is placed below the marker. Eighty percent of all x data are left of the dashed vertical lines; the dashed slopes represent unity.

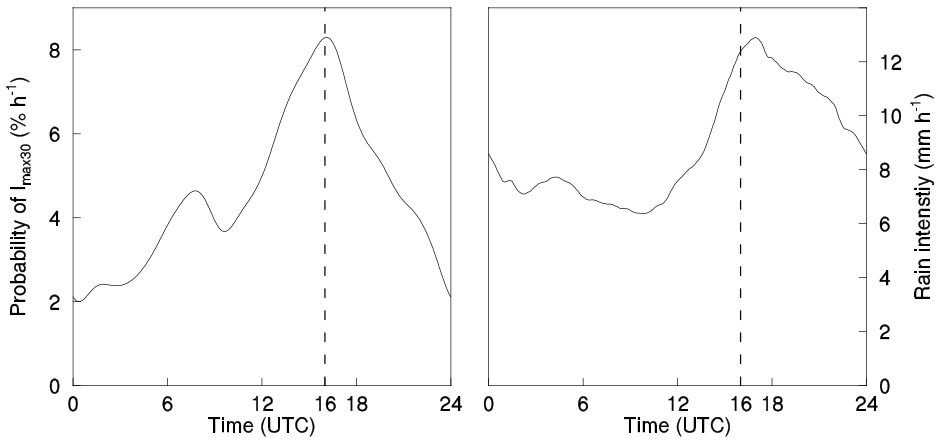

Fig. 3. The diurnal variation in the probability of the occurrence of I_{max30} (left panel) and in the rain intensity (right panel) during the rain period of all 605737 erosive events.

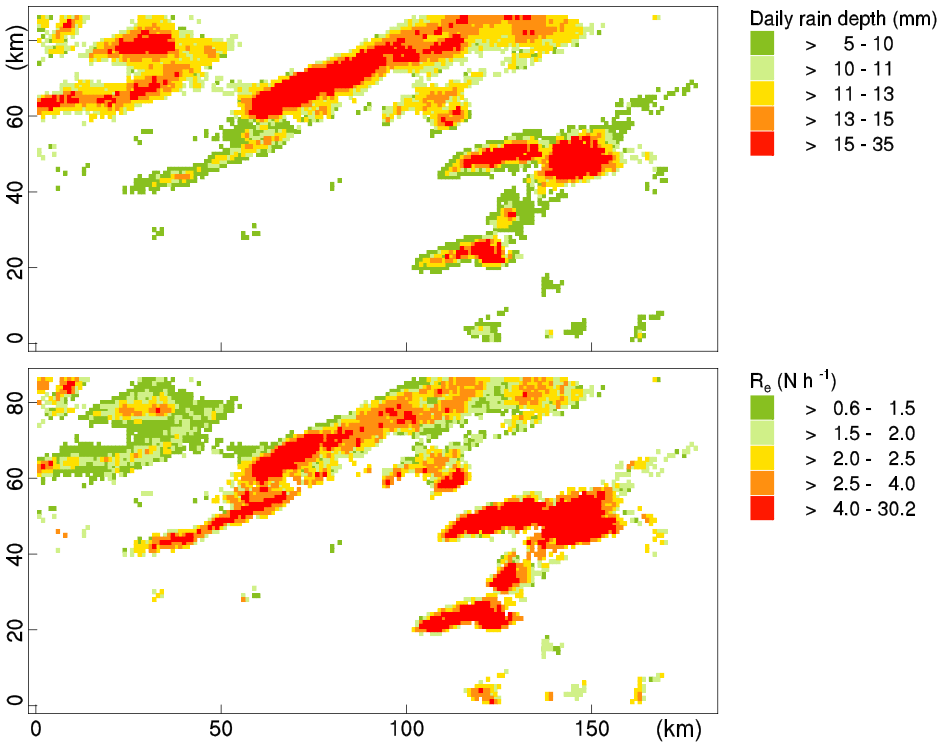

Fig. 4. Daily rain depth (upper panel) and R_e (lower panel) on 12 May 2011 for grid cells with $R_e > 0$; each color occupies the same spatial proportion (ranges limited by quintiles).

3.3. Effect of adjustment

For a subset of 19 typical erosive days comprising a total of 93 456 erosive events, daily rain depth, I_{max30}, kinetic energy and R_e, were lower than 24.0 mm d^{-1}, 16.3 mm h^{-1}, 0.5 kJ m^{-2} and 7.2 N h^{-1} respectively in 80% of all cases (80th percentile; see Fig. 2 for daily rain depth and R_e). These values slightly increased or remained unchanged when adjusted (compare data derived from RW and RY in Fig. 2). Most of the values of R_e accumulated in the lowest class of R_e in Fig. 2. While average daily rain depth of the lowest class was increased by adjustment, the average of R_e in the lowest class was not significantly changed by adjustment. However, the standard deviation was as large as the mean indicating adjustment had a large effect for the individual events. As the average increased, the standard deviations increased pronouncedly, especially for R_e. A R_e of 200 N h^{-1} for the original RY data, for example, could yield values between 100 N h^{-1} and 300 N h^{-1} after adjustment (as quantified by the 95% interval of the population). The effect of adjustment on the average then changed around the 80th percentile above which the averages were lowered by adjustment. This effect increased with increasing averages and was stronger for R_e as the effect was squared by the multiplication of I_{max30} and the kinetic energy. In relation to the regional long-term R factor of 70 N h^{-1}, the difference between R_e estimated from original RY data and from adjusted (to preserve hourly rain-gauge rainfall) RW data was mainly (75% of all erosive events) between −3% and 2% but was in the extremes −225% and 283%.

3.4. Diurnal variation of erosive-rain properties

Intensities during the rain period of erosive days showed a clear diurnal variation with a positively skewed peak in mean intensity between 15:00 and 24:00, which then also applied for the diurnal variation in kinetic energy. Not surprisingly, the maximum proba-

Table 2
Spatial properties of daily rain depth and event erosivity derived from anisotropic variograms along the short axis of 170 erosive days.

		Range	S[a]	sqrt(S)	pS[b]	pCV[c]	Gradient[d]	Rel. gradient[e]
Rain depth	Unit	km	$mm^2\ d^{-2}$	$mm\ d^{-1}$	%	%	$mm\ d^{-1}\ km^{-1}$	$\%\ km^{-1}$
	Min	2.0	1	0.6	31	4	0.03	0.3
	Mean	13.2	19	3.7	96	26	0.43	3.5
	Max	77.0	205	14.3	100	67	1.97	14.3
Erosivity	Unit	km	$N^2\ h^{-2}$	$N\ h^{-1}$	%	%	$N\ h^{-1}\ km^{-1}$	$\%\ km^{-1}$
	Min	1.9	1	0.2	29	9	0.01	0.8
	Mean	9.7	34	3.6	95	77	0.59	13.3
	Max	58.9	1141	33.8	100	345	3.09	51.1

[a] S: total sill.
[b] pS: partial sill relative to total sill.
[c] pCV: partial coefficient of variation (=sqrt(S)*pS/mean).
[d] Gradient = sqrt(S)*pS/range.
[e] Relative gradient: gradient relative to mean rain depth or mean erosivity.

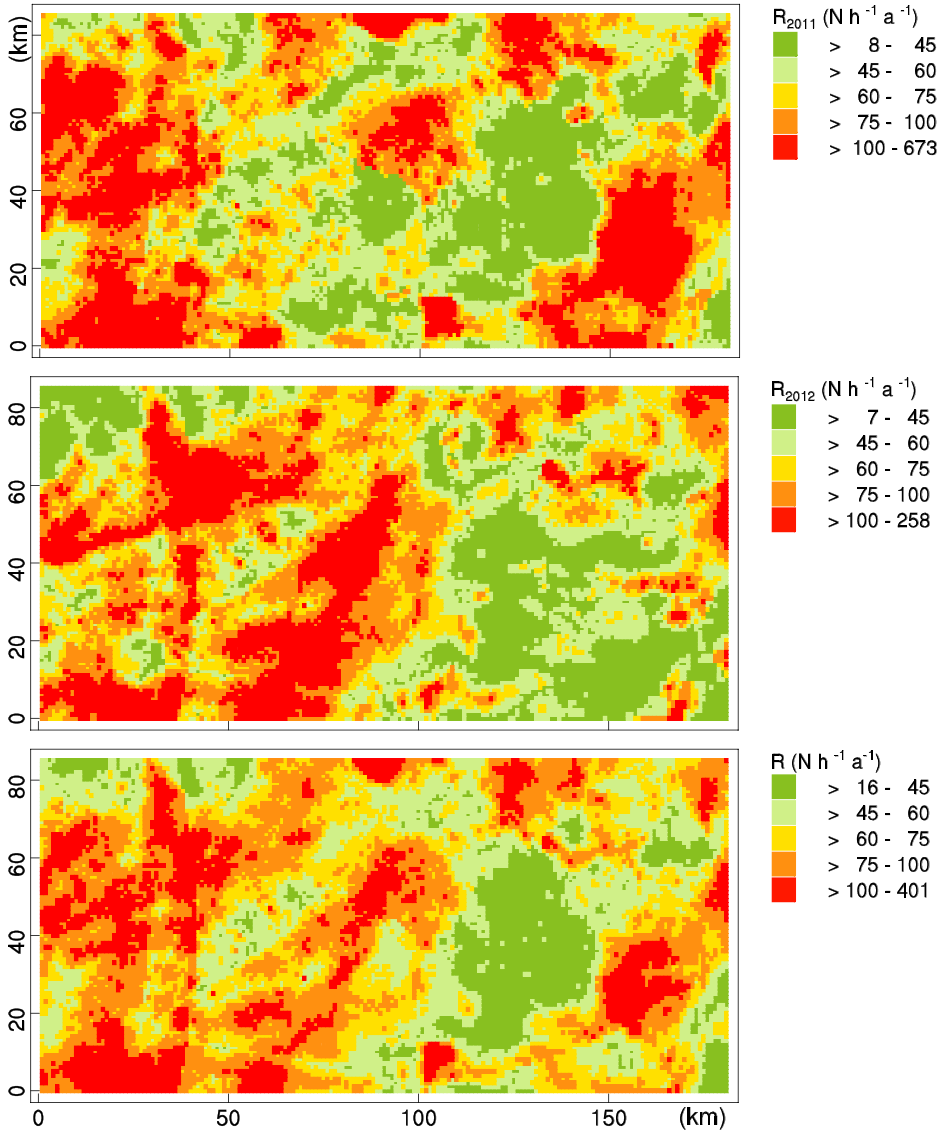

Fig. 5. Annual sum of R_e for 2011 (upper panel) and 2012 (middle panel) and biennial mean R (lower panel); each color occupies the same spatial proportion (ranges limited by quintiles) for the combined maps.

bility of I_{max30} occurrence was on the left side of this peak at around 16:00 (17:00 local time). At this time the probability was about four times higher than around midnight when the probability was lowest (Fig. 3). Thus, the diurnal variation in probability was much more pronounced than the variation in intensity.

Dry spells that met the criterion of the R factor for separation into different rains were quite common (24% of all erosive events). Probability of a dry spell was highest in the morning hours. In most cases only one of both rains separated by a dry spell met the criteria to be erosive. Hence in the majority of cases the dry spells

Table 3
Mean spatial properties of erosivity along the short axis for 81 erosive days in 2011 and 89 erosive days in 2012 for grid cells with $R_e > 0$ and their annual sum and the biennial mean; the gradient is the square root of the partial sill divided by the range.

Erosive day	Nugget ($N^2\ h^{-2}$)	S[a] ($N^2\ h^{-2}$)	pS[b] (%)	Range (km)	Gradient[c] ($N\ h^{-1}\ km^{-1}$)
Event mean 2011	0.1	45	96	9.8	0.7
Annual sum 2011	29.9	1557	98	21.8	1.8
Event mean 2012	0.3	24	94	9.6	0.5
Annual sum 2012	20.2	917	98	20.5	1.4
Biennial mean	19.5	759	97	21.6	1.2

[a] S: total sill.
[b] pS: partial sill relative to total sill.
[c] Gradient = sqrt(S)*pS/range.

caused the erosive event to be shorter and have 25% less rain than daily rainfall. On the other hand, 36% of all erosive events extended beyond midnight. In these cases the erosive event was longer and had more rainfall then the daily rainfall (when separated at 0:00 UTC). Consequently, in 50% of all cases daily rainfall was not identical to erosive rainfall but the errors operated in opposite direction.

3.5. Spatial structure of erosive rains and rain erosivities

3.5.1. Single events

Erosive cells were anisotropic in 96% of all cases (for example see Fig. 4). The directions of the short axis were almost evenly distributed. The short axis should characterize the diameter of a rain cell while the long axis is determined by the movement of a rain cell and its life-time. The short axis was oriented N-S in 26% of all cases, NE-SW in 24%, E-W in 20% and NW-SE in 26%. Thus, a preferential direction of wind during erosive rains was not evident for the sum of rains while it was pronounced for many individual rains (e.g., Fig. 4). The average range of R_e was 9.3 km on the short axis and 49.2 km on the long axis and thus differences were rather large. Only the semivariograms along the short axis will be reported because they quantify the maximum gradients of autocorrelation and the size of the erosive cells. The nugget was usually unimportant (on average less than 1% of the total sill). A Gaussian model was appropriate in 6% of all cases. A Gaussian model evolves when gradients within the center of a rain cell are small or when a large fringe of low erosivity and hence low gradient surrounds the rain cell. More often a hole effect was present (67% along the short axis) indicating that areas covered by the majority of rain cells did not overlap and had a diameter along the short axis of twice the range.

R_e occurred with higher variation and in smaller cells than daily rain depth. Ranges of autocorrelation were about 3 km (equal to about 30%) longer for daily rain depth than for R_e (Table 2) and thus erosivity cells covered only 74% of (erosive) rain cells. Within these ranges, the gradients (change per km) of R_e relative to the mean R_e of the erosive day were about four times steeper than the gradients of daily rain depth. Partial sills relative to the mean were about three times higher for R_e than for daily rain depth (Table 2). Local gradients relative to the mean were considerably steeper with 22% km^{-1} (0.8 $N\ h^{-1}\ km^{-1}$) for R_e and 6% km^{-1} (0.9 $mm\ d^{-1}\ km^{-1}$) for daily rain depth and became even steeper when only the maximum gradient to one of the eight neighbors was considered. Then, for R_e, the gradient was 33% km^{-1} (1.1 $N\ h^{-1}\ km^{-1}$) and 10% km^{-1} (1.3 $mm\ d^{-1}\ km^{-1}$) for daily rain depth. Adjacent cells differed by up to 120 $N\ h^{-1}\ km^{-1}$ and 26 $mm\ d^{-1}\ km^{-1}$. All analyses thus indicated that a much higher spatial data density is necessary to determine the spatial variation of R_e then that of rainfall.

Exemplarily, the erosive rain on 12 May 2011 (Fig. 4) showed similar spatial structures for I_{max30}, kinetic energy and daily rain depth. The highest values of each parameter were in the same geographical area. The relative gradients increased from daily rain depth (3% km^{-1}) to kinetic energy (5% km^{-1}) to I_{max30} (7% km^{-1}) but remained less than half of the relative gradient of R_e (17% km^{-1}). The ranges were similar for daily rain depth and kinetic energy (8.6 km and 7.7 km), while the range of I_{max30} was considerably shorter and identical to that of R_e (6.1 km), indicating that the differences in the pattern properties between R_e and daily rain depth mainly resulted from I_{max30} reflecting short bursts of high intensity in the rain. The relation between these parameters behaved essentially similarly on the other erosive days even though the absolute values differed considerably between rains (Table 2).

3.5.2. Annual sum

The patchy structure of erosivity remained when all R_e of all erosive days of a year were combined in R_{year} maps (Fig. 5 upper and middle panel). Even the biennial average (Fig. 5 lower panel) still exhibited a pronounced patchy structure with large deviations from the expected long-term mean. Due to the almost even distribution of anisotropy among cardinal directions, no prevailing wind direction shaped the patchy structure of the annual sums of erosive rain. Also orographic rain, which could be expected to influence the right edge of the research area due to a mountain ridge adjoining to the east, was not overriding the patchy structure.

The sill of annual maps increased compared to the sill of event maps due to the partial overlap of cells from different rains (Table 3). The range also became larger for the annual sums than for the individual events. Due to the larger increase in sill than in range, the mean gradient for the annual maps was about twice as large as the average of the gradients for the individual erosive rainfalls that contributed to the annual map (Table 3). The nugget was unimportant and contributed less than 5% to the total sill in all cases.

The biennial average R still had a spread of values similar to the annual maps, indicating that many years will be necessary for the patchiness to level out. The highest biennial value (401 $N\ h^{-1}\ a^{-1}$) was still almost 6 times higher than the expected areal average of about 70 $N\ h^{-1}\ a^{-1}$ although the biennial average of the entire area (73 $N\ h^{-1}\ a^{-1}$) was close to this expected mean. The areal extension of the middle class in Fig. 5 (60–75 $N\ h^{-1}\ a^{-1}$), in which the long-term mean can be expected, increased only by 4% while the lowest and highest classes, which should disappear in the long-term mean, were reduced by 8% and 4%. Thus, many years will be necessary to reveal the long-term pattern of this landscape segment.

4. Discussion

The RADOLAN data revealed a very high spatial variability in erosivity of individual rains, which agrees with other studies (Angulo-Martínez et al., 2009; Fiener and Auerswald, 2009). This was not only caused by the higher spatial variability of rains >10 mm compared to average rains (Einfalt et al., 1998). The spatial range of R_e cells was only 74% of the spatial range in daily rain depth even when only erosive rains were considered that usually yielded more than 10 mm of rain. The erosivity cells covered on average only 35% of the area of the corresponding rain cells (assuming a circular cell with a radius equal to the mean short-axis

range). As a consequence, gradients of rain erosivity were much steeper than gradients in rain depth. This result was not unexpected given that rain erosivity is derived from the multiplication of two rain properties, which depend on rain intensity and thus, any gradient in rain intensity will appear squared in rain erosivity. More surprisingly, these steep spatial gradients persisted when all erosive rains in a year were accumulated to yield the annual or biennial erosivity maps. This result was an effect of the steep gradients, which can only evolve when the cells of erosive rains are small. As a consequence of the small extension of erosive rain cells, even the biennial erosivity map exhibited a pronounced heterogeneity. Large areas still existed where total rain erosivity was less than half of the expected long-term mean, while within 50 km distance annual erosivity was more than twice the expected long-term mean. Therefore, much longer time periods than two years are necessary to level out the spatial variability created by individual events. Rain erosivity data with a high spatial resolution will hence be indispensable for many questions in erosion research and consulting. RADOLAN data since 2000 will become available in the near future and allow answering the question whether 15 years are sufficient to level out the patchy structure and to reveal weak influences like orographic rainfall, which can be expected to exist. A smaller number of years may be necessary in regions characterized by a large number of erosive rains (Gonzalez-Hidalgo et al., 2012) but this effect could be opposed by steeper gradients of erosivity cells. These gradients seem to become considerably steeper in regions with frequent erosive rains (Fiener and Auerswald, 2009).

The different equations of kinetic energy had a negligible influence on erosivity compared to the pronounced spatial variability. Regionalization of such equations by measuring drop sizes distribution under a variety of climates (e.g., Cerdà, 1997) are necessary under a scientific point of view but erosion prediction for practical purposes will profit more from a higher spatial resolution of rain data. The steep gradients within individual rains are likely responsible in part for the large variability in soil loss between replicated plots (Nearing et al., 1999), which presently restricts the development of better models because assuming homogeneity in rainfall adds a large unexplained variance.

Adjacent cells had gradients of up to 120 N h^{-1} km^{-1}. In extreme cases, rain-gauge measurements may thus only be valid for the distances considerably shorter than 1 km around a rain gauge, although on average the RMSE between rain-gauge and radar measurements was only 3 mm. Shorter distances can be achieved in erosion plot experiments but not in many other cases. RADOLAN delivers for the first time rain data with enough spatial detail to meet the requirements of regional erosion research while point measurements (rain gauges) or spatial data of lower resolution (older radar products) are strongly restricted in their applicability. The question arises of whether an even finer spatial resolution than that of RADOLAN is necessary. The minimum range along the short axis of the semivariograms was 2 km and the mean range was 10 km, indicating that beyond the resolution of RADOLAN (1 km) the gradients were near to linear. This agreed with the results of Fiener and Auerswald (2009), who had set up a dense rain-gauge network within 1 km^2. Half of their erosive rains had strong gradients in rain erosivity. All of their gradient rains followed linear semivariograms and indicated that the erosive cell extended considerably beyond their research area. From our findings and those of Fiener and Auerswald (2009), we can safely assume that erosivity changes almost linearly between two opposite sides within a RADOLAN cell. Consequently, each RADOLAN cell delivers an unbiased estimate of the average erosivity of all locations within this cell. Further, for applications of rain erosivity that require a higher spatial resolution than that of RADOLAN cells, a linear interpolation of rain erosivity between neighboring RADOLAN cells should yield acceptable estimates.

The rain fields of erosive rains usually showed a pronounced anisotropy, which resulted from the movement of rain cells, as indicated from the temporal shift in rain (data not shown). This movement is advantageous because it levels out differences between rain cells and their neighborhood. Fiener and Auerswald (2009) had already noted that the highest erosivities occurred when the movement of the rain cell was slow.

Our data showed that the adjustment of radar data is indispensable, especially when these data are used for calculation of rain erosivity, because any error will appear squared in erosivity although the effect on average rainfall was negligible. We found that without adjustment rain erosivities of 100 N h^{-1} and 300 N h^{-1} could not be distinguished. The difference of 200 N h^{-1} is equivalent to the three-year sum of the long-term average erosivity. In consequence, radar data without ground-truth adjustment should not even be used to estimate long-term averages of rain erosivity. In RADOLAN, radar estimates are adjusted hourly but it is expected that the quality of the 5-min radar data will approach the quality of the 60-min data in the near future (Helmert et al., 2014).

Still, our analysis showed that an hourly adjustment was adequate even for the calculation of erosivity because the calculation of kinetic energy was almost independent of the temporal resolution within this time span and the adjustment should also be applicable for I_{max30} as I_{max30} comprised 80% of the hourly rainfall. The influence on kinetic energy is small because total kinetic energy increases almost linearly with intensity ($r^2 = 0.9998$ with a linear regression) between 0 mm h^{-1} and 100 mm h^{-1}. This is due to the large effect of the increasing amount of rain that overrides the comparably small effect of changing energy per mm of rain as derived from Eq. (2). In consequence, a deviation of a 5 min increment cannot have a large effect if it is compensated by another increment and thus does not show up in the hourly adjustment factor. The effect will be strongest at the upper boundary of Eq. (2a) but even there the effect is small. Two 5 min increments that deliver a constant intensity of 76.3 mm h^{-1} will yield $E = 0.36$ kJ m^{-2}. A large error in the adjustment factor that causes both intensities to be 50 mm h^{-1} and 102.6 mm h^{-1} would lead to $E = 0.43$ kJ m^{-2}. The intensity was between 60 mm h^{-1} and 90 mm h^{-1}, where such an error may be relevant, only in 0.05% of all cases. The error in I_{max30} can be larger. However, I_{max30} contributed on average 80% to the hourly rainfall. Hence, most of the hourly adjustment factor must have evolved during the period of I_{max30} and be valid for I_{max30}.

The high spatio-temporal resolution, which is necessary for erosivity calculations, requires an enormous data volume and data processing. In our analysis a temporal resolution of 5 min appeared to be adequate for the calculation of erosivity and caused only a bias, compared to tipping-bucket resolution, that was several orders of magnitude lower than the variation between adjacent cells.

Erosivity exhibited a pronounced diurnal variation. Rain intensity peaked at 17:00 UTC (=18:00 Central European Time). This agrees with the earlier finding that rainfall maximum is at around 18:00 (Paulat et al., 2008) and relates to the mainly convective origin of erosive rains.

5. Conclusions

Spatio-temporal variability of erosivity was considerably stronger than that of daily rain depth. This calls for an area-wide collection of rainfall data at high spatio-temporal resolution, such as that provided by RADOLAN. Typical densities of rain gauges clearly miss many high-erosivity rain cells. The complete coverage and high spatio-temporal resolution of radar measurements supersedes the need to extrapolate erosivity obtained from sparse but intensity-recording rain gauges by making use of spatially denser data of coarser temporal resolution (e.g., Yin et al., 2015), satellite

data (Vrieling et al., 2010; Vrieling et al., 2014) or long-term precipitation maps (e.g. Rogler and Schwertmann, 1981; Strauss et al., 1995). The RADOLAN-derived erosivities could be a valuable source for validating larger-scale coarse-resolution erosivity assessments that are still justified in areas where radar data of similar quality to RADOLAN are not available.

Adjustment of radar data was indispensable because the errors in R_e would not level out even in long-term averages. Hourly adjustment seemed sufficient for the calculation of R_e.

Acknowledgements

This study was part of the project "Ermittlung des Raum- und Jahreszeitmusters der Regenerosivität in Bayern aus radargestützten Niederschlagsdaten zur Verbesserung der Erosionsprognose mit der Allgemeinen Bodenabtragsgleichung" at the Bavarian State Research Center for Agriculture funded by the Bayerisches Staatsministerium für Ernährung, Landwirtschaft und Forsten. We acknowledge many helpful comments by Anton Vrieling and Artemi Cerdà and language editing by Karin Levin.

References

Angulo-Martínez, M., López-Vicente, M., Vicente-Serrano, S.M., Beguería, S., 2009. Mapping rainfall erosivitiy at a regional scale: a comparison of interpolation methods in the Ebro Basin (NE Spain). Hydrol. Earth Syst. Sci. 13, 1907–1920.

Auerswald, K., Fiener, P., Dikau, R., 2009. Rates of sheet and rill erosion in Germany—A meta-analysis. Geomorphology 111, 182–193.

Auerswald, K., 2006. Germany. In: Boardman, J., Poesen, J. (Eds.), Soil Erosion in Europe. Wiley, pp. 213–230 (Chapter 1.18).

Bartels, H., Weigl, E., Reich, T., Lang, P., Wagner, A., Kohler, O., Gerlach, N., 2004. MeteoSolutions GmbH, Projekt RADOLAN: Routineverfahren zur Online-Aneichung der Radarniederschlagsdaten mit Hilfe von automatischen Bodenniederschlagsstationen (Ombrometer) DWD.

Borga, M., 2002. Accuracy of radar rainfall estimates for streamflow simulation. J. Hydrol. 267, 26–39.

Bronstert, A., Bárdossy, A., 2003. Uncertainty of runoff modelling at the hillslope scale due to temporal variations of rainfall intensity. Phys. Chem. Earth 28, 283–288.

Cerdà, A., 1997. Rainfall drop size distribution in the Western Mediterranean basin Valencia, Spain. Catena 30, 169–182.

Crum, T.D., Saffle, R.E., Wilson, J.W., 1998. An update on the NEXRAD program and future WSR-88D support to operations. Weather Forecasting 13, 253–262.

Cruse, R., Flanagan, D., Frankenberger, J., Gelder, B., Herzmann, D., James, D., Krajewski, W., Kraszewski, M., Laflen, J., Opsomer, J., Todey, D., 2006. Daily estimates of rainfall, water runoff, and soil erosion in Iowa. J. Soil Water Conserv. 61, 191–199.

Da Silva, R.M., Guimarães Santos, C.A., de Lima Silva, V.C., e Silva, L.P., 2013. Erosivity, surface runoff, and soil erosion estimation using GIS-coupled runoff-erosion model in the Mamuaba catchment, Brazil. Environ. Monit. Assess. 185, 8977–8990.

Datta, S., Jones, W.L., Roy, B., Tokay, A., 2003. Spatial variability of surface rainfall as observed from TRMM field campaign data. J. Appl. Meteorol. 42, 598–610.

Einfalt, T., Johann, G., Pfister, A., 1998. On the spatial validity of heavy point rainfall measurements. Water Sci. Technol. 37, 21–28.

Faurès, J.-M., Goodrich, D.C., Woolhiser, D.A., Sorooshian, S., 1995. Impact of small-scale spatial rainfall variability on runoff modeling. J. Hydrol. 173, 309–326.

Fiener, P., Auerswald, K., 2009. Spatial variability of rainfall on a sub-kilometre scale. Earth Surf. Processes Landf. 34, 848–859.

Foster, G.R., 2008. Draft: science documentation. In: Revised Universal Soil Loss Equation version 2 (RUSLE2). USDA-Agricultural Research Service, Washington, D.C.

Gonzalez-Hidalgo, J.C., Batalla, R.J., Cerda, A., de Luis, M., 2012. A regional analysis of the effects of largest events on soil erosion. Catena 95, 85–90.

Gryschka, M., Witha, B., Etling, D., 2008. Scale analysis of convective clouds. Meteorol. Z. 17, 785–791.

Hardegree, S.P., Van Vactor, S.S., Levinson, D.H., Winstral, A.H., 2008. Evaluation of NEXRAD radar precipitation products for natural resource applications. Rangel. Ecol. Manag. 61, 346–353.

Helmert, K., Tracksdorf, P., Steinert, J., Werner, M., Frech, M., Rathmann, N., Hengstebeck, T., Mott, M., Schumann, S., Mammen, T., 2014. DWDs new radar network and post-processing algorithm chain. In: 8th European Conference on Radar in Meteorology and Hydrology (ERAD), Garmisch-Partenkirchen.

Hengstebeck, T., Helmert, K., Seltmann, J., 2010. RadarQS – a standard quality control software for radar data at DWD. In Proc. 6th European Conference on Radar in Meteorology and Hydrology (ERAD).

Journel, A.G., Huijbregts, C.J., 1978. Mining Geostatistics. Academic Press, pp. 600.

Kirkby, M.J., Bracken, L.J., Shannon, J., 2005. The influence of rainfall distribution and morphological factors on runoff delivery from dryland catchments in SE Spain. Catena 62, 136–156.

Kruizinga, S., Yperlaan, G.J., 1978. Spatial interpolation of daily totals of rainfall. J. Hydrol. 36, 65–73.

Lu, H., Yu, B., 2002. Spatial and seasonal distribution of rainfall erosivity in Australia. Aust. J. Soil Res. 40, 887–901.

Malkowski, G., 1961. Über die absolute Dauer konvektiver Starkregen. Archiv für Meteorologie. Geophysik und Bioklimatologie, Serie A 12, 376–381.

Malkowski, G., 1965. Zur Abhängigkeit der Schauergröße von der vertikalen Windverteilung. Archiv für Meteorologie. Geophysik und Bioklimatologie, Serie A 14, 441–448.

Nearing, M.A., Govers, G., Norton, L.D., 1999. Variability in soil erosion data from replicated plots. Soil Sci. Soc. Am. 63, 1829–1835.

Nearing, M.A., 1998. Why soil erosion models over-predict small soil losses and under- predict large soil losses. Catena 32, 15–22.

Paulat, M., Frei, C., Hagen, M., Wernli, H., 2008. A gridded dataset of hourly precipitation in Germany: its construction, climatology and application. Meteorol. Z. 17, 719–732.

Pebesma, E.J., 2004. Multivariable geostatistics in S: the gstat package. Computers Geosci. 30, 683–691.

Quirmbach, M., Schultz, G.A., 2002. Comparison of rain-gauge and radar data as input to an urban rainfall-runoff model. Water Sci. Technol. 45 (2), 27–33.

R Development Core Team, 2014. R: A Language and Environment for Statistical Computing. R Foundation for Statistical Computing, Vienna, Austria http://www.R-project.org/.

Rogler, H., Schwertmann, U., 1981. Erosivität der Niederschläge und Isoerodentkarte Bayerns. Zeitschrift für Kulturtechnik und Flurbereinigung 22, 99–112.

Sadeghi, S.H.R., Moatamednia, M., Behzadfar, M., 2011. Spatial and temporal variations in the rainfall erosivity factor in Iran. J. Agric. Sci. Technol. 13, 451–464.

Seo, D.-J., Seed, A., Delrieu, G., 2010. Radar and multisensor rainfall estimation for hydrologic applications. Geophys. Monogr. Ser. 191, 79–104.

Sideris, I.V., Gabella, M., Erdin, R., Germann, U., 2014. Real-time radar—rain-gauge merging using spatio-temporal co-kriging with external drift in the alpine terrain of Switzerland. Q. J. R. Meteorol. Soc. 140, 1097–1111.

Silverman, B.W., 1986. Density estimation for statistics and data analysis. In: Monographs on Statistics and Applied Probability. Chapman and Hall, London.

Strauss, P., Auerswald, K., Klaghofer, E., Blum, W.E.H., 1995. Erosivität von Niederschlägen, ein Vergleich Österreich—Bayern. Zeitschrift für Kulturtechnik und Landentwicklung 36, 304–308.

Syed, K.H., Goodrich, D.C., Myers, D.E., Sorooshian, S., 2003. Spatial characteristics of thunderstorm rainfall fields and their relation to runoff. J. Hydrol. 271, 1–21.

Tsanis, I.K., Gad, M.A., Donaldson, N.T., 2002. A comparative analysis of rain-gauge and radar techniques for storm kinematics. Adv. Water Resour. 25, 305–316.

Vrieling, A., Sterk, G., de Jong, S.M., 2010. Satellite-based estimation of rainfall erosivity for Africa. J. Hydrol. 395, 235–241.

Vrieling, A., Hoedjes, J.C.B., van der Velde, M., 2014. Towards large-scale monitoring of soil erosion in Africa: accounting for the dynamics of rainfall erosivity. Glob. Planet. Change 115, 33–43.

Weigl, E., 2011. Verifikation, Aneichstationsdichte und Ombrometerverfügbarkeit. Newsl. Hydrometeorologie 6, 4–13.

Weigl, E., Winterrath, T., 2009. Radargestützte Niederschlagsanalyse und—vorhersage (RADOLAN, RADVOR-OP). Promet 35, 78–86.

Weusthoff, T., Hauf, T., 2008. Basic characteristics of post-frontal shower precipitation rates. Meteorol. Z. 17, 793–805.

Wischmeier, W.H., Smith, D.D., 1958. Rainfall energy and its relationship to soil loss. Trans. Am. Geophys. Union 39, 285–291.

Wischmeier, W.H., Smith, D.D., 1978. Predicting rainfall erosion losses. In: Agricultural Handbook 537. USDA, Science and Education Administration, Washington, DC.

Wohlrab, B., Ernstberger, H., Meuser, A., Sokollek, V., 1992. Landschaftswasserhaushalt: Wasserkreislauf und Gewässer im ländlichen Raum; Veränderungen durch Bodennutzung, Wasserbau und Kulturtechnik. Parey-Verlag, Hamburg, Berlin.

Yang, X., Yu, B., 2015. Modelling and mapping rainfall erosivity in New South Wales, Australia. Soil Res. 53, 178–189.

Yin, S., Xie, Y., Liu, B., Nearing, M.A., 2015. Rainfall erosivity estimation based on rainfall data collected over a range of temporal resolutions. Hydrol. Earth Syst. Sci. 19, 4113–4126.